Desalination 249 (2009) 1048–1054

Contents lists available at ScienceDirect

Desalination

journal homepage: www.elsevier.com/locate/desal

Characterization of the uptake of aqueous Ni^{2+} ions on nanoparticles of zero-valent iron (nZVI)

Nazlı Efecan [a], Talal Shahwan [a,b,*], Ahmet E. Eroğlu [a], Ingo Lieberwirth [c]

[a] Department of Chemistry, İzmir Institute of Technology, Urla 35430, İzmir, Turkey
[b] Department of Chemistry, Birzeit University, Ramallah, West Bank, Palestine
[c] Max Planck Institute for Polymer Research, Mainz, Germany

ARTICLE INFO

Article history:
Accepted 21 June 2009
Available online 7 October 2009

Keywords:
Nano zero-valent iron
Uptake
Ni^{2+}

ABSTRACT

This study investigates the fixation of aqueous Ni^{2+} ions by nanoparticles of zero-valent iron (nZVI) prepared using the borohydride reduction method. The uptake of Ni^{2+} was tested under various experimental conditions like initial concentration, time, pH, and repetitive application of nZVI. Part of the experiments was devoted to comparing the extent of uptake of Ni^{2+} ions with those of Cu^{2+}, Cd^{2+}, Zn^{2+}, and Sr^{2+} ions, which belong to a wide range of standard reduction potentials. Particle size analysis of nZVI in aqueous solution indicated that the material suffered extensive aggregation, much above the extent of aggregation known for dry nZVI. Nevertheless, nZVI showed fast uptake kinetics and very high uptake capacity. The overall results demonstrated the high fixation capability of nZVI towards the studied transition metal ions in aqueous solution. The same conclusion is, however, not valid for the removal of Sr^{2+} ions.

1. Introduction

Zero-valent iron nanotechnology is an emerging environmental technology that is suggested to convey cost effective solutions for *in situ* and *ex situ* remediation [1]. By virtue of their high surface/volume ratios, nanoparticles of zero-valent iron (nZVI) possess enormous amount of energy that brings about a high sequestration capacity and provide a kinetic advantage in the uptake process [2]. Although the application of iron nanoparticles suffers from some still unresolved uncertainties, the material is being accepted as a versatile tool for the remediation of different organic and inorganic environmental pollutants [3]. The topic of metal ion retention by nZVI is an expanding area that has been handled by various research groups during the last decade. The effectiveness of nZVI for the removal of Co^{2+} and Cu^{2+} ions from aqueous solutions has been recently reported by our group [4–6]. The applicability of nZVI and nZVI-based materials for the fixation of different metal cations (like As, Cu, Co, Pb, Cd, etc.) and some anions (like chromate and nitrate) has been documented in literature in a number of previous works [e.g. 7–13]. This area continues to extend in the direction of enhancing the properties of nZVI and gaining better understanding for the mechanism of interaction.

Heavy metals are among the priority pollutants as they are not biodegradable, and consequently can accumulate in the environment causing potential short term and long term hazards [14]. Nickel, is a heavy metal that is used in manufacturing alloys, stainless steel, and in plating. The discharge of this element into the aqueous environment will bring about detrimental effects on the biosphere. The retention of Ni^{2+} ions on nZVI was reported in a previous study that investigated the topic from a mechanistic view point [15]. To our knowledge, no detailed study on the effect of various experimental parameters on the extent of Ni^{2+} uptake by nZVI is available in literature.

This work aimed at investigating the mechanism of uptake of Ni^{2+} on nZVI, studying the extent of uptake as a function of concentration, time, pH, and repetitive application of nZVI. Desorption tests were also performed to test the stability of uptake. Another part of the experiments was devoted to comparing the extent of uptake of Ni^{2+} ions with those of Cu^{2+}, Cd^{2+}, Zn^{2+}, and Sr^{2+} ions, which belong to a wide range of standard reduction potentials. The relevant experiments aimed at investigating possible correlation between the extent of uptake and the standard reduction potentials for the studied cations. The aqueous concentration of Ni and the other elements was determined using Flame Atomic Absorption Spectrometry (FAAS). The synthesized nZVI material was characterized using Zeta meter, BET-N_2, scanning electron microscopy/energy dispersive X-ray analysis (SEM/EDX), high resolution-transmission electron microscopy (HR-TEM), X-ray photoelectron spectroscopy (XPS), and X-ray diffraction (XRD).

* Corresponding author. Current Address: Department of Chemistry, Birzeit University, Ramallah, West Bank, Palestine.
E-mail addresses: talalshahwan@iyte.edu.tr, tshahwan@birzeit.edu (T. Shahwan).

0011-9164/$ – see front matter © 2009 Elsevier B.V. All rights reserved.
doi:10.1016/j.desal.2009.06.054

2. Experimental

2.1. Preparation of nZVI

The synthesis of nZVI was performed using the method of liquid-phase reduction utilizing $NaBH_4$ (Aldrich 4511-2) as the reducing agent. The applied procedure was reported in detail in our earlier works [e.g. 4]. In brief, a 17.8 g sample of $FeCl_2 \cdot 4H_2O$ (Sigma-Aldrich 22029-9) was dissolved in 50.0 mL solution of absolute ethanol (Riedel-de Haën 32221) and distilled water (4:1 v/v). An 8.47 g $NaBH_4$ was separately dissolved in 220 mL of distilled water. $NaBH_4$ solution was then added to a Fe^{2+} solution drop wise while providing well-stirring to the reaction mixture. After the addition of all the $NaBH_4$ solution, the mixture was mixed for extra 20 min period. The iron powder was then separated from the solution by vacuum filtration, and the filtrate was washed at least three times with 99% absolute ethanol. The powder was dried in the oven at 75 °C overnight under atmospheric oxygen.

2.2. Characterization techniques

The solid samples were characterized using XPS, XRD, HR-TEM and SEM/EDX. In the XPS analysis, the samples were analyzed under high vacuum ($<1\times10^{-7}$ mbar) in a Thermo Fisher Scientific Escascope X-ray photoelectron spectrometer equipped with a dual anode. The anode X-rays consisted of Al-K_α radiation at 400 W (15 kV). The analysis of the data was realized using Pisces (Dayta Systems, UK) software. The XRD analysis was performed using a Philips X'Pert Pro instrument in which the source consisted of Cu K_α radiation ($\lambda = 1.54$ Å). SEM/EDX analysis was carried out using a Philips XL-30 S FEG type instrument. The nZVI samples were sprinkled onto adhesive carbon tapes supported on metallic disks, and their images and elemental contents were recorded at different magnifications. HR-TEM analysis was done using a Tecnai F20. The instrument was operated at 200 kV acceleration voltages. Prior to analysis, the nZVI sample was dispersed in ethanol using an ultrasonic bath. Subsequently, a drop of the dispersion was applied to a holey carbon TEM support grid and excess solution was blotted off by a filter paper.

The particle size analysis of nZVI was performed using a Malvern Mastersizer 2000 instrument. For this purpose, 2.5 g of nZVI was dipersed in 25 mL of Millipore water (18.2 MΩ) and the mixture was introduced to the instrument in small portions. Additional water was added to the suspension whenever required to increase the signal intensity, while subjecting the mixtures to ultrasonic shaking.

The surface area of the nZVI samples was determined by the BET-N_2 method using a Micromeritics Gemini 5 instrument. The iso-electric-point (IEP) of nZVI was determined using a Zeta-Meter 3.0 instrument. The zeta potential was measured for a series of suspensions in the pH range 6.0–12.0, at a concentration of 0.1 g/L.

2.3. Uptake experiments

Throughout these experiments, the aqueous Ni^{2+} solutions were prepared by dissolving appropriate amounts of $NiCl_2.6H_2O$ (Carlo Erba 464645) in high purity water (Millipore, 18.2 Ω). All the experiments were carried out at ambient temperature and pressure using 50.0 mL falcon tubes. The contents of the tubes were mixed on an orbital shaker operating at 350 rpm, and were subsequently centrifuged at 6000 rpm at the end of the uptake experiments. The supernatant solutions were filtered and transferred into clean falcon tubes and acidified with concentrated nitric acid (1% v/v), and were then analyzed using a Thermo Elemental SOLAAR M6 Series atomic absorption spectrometer with air-acetylene flame.

The experiments were performed in duplicate sets and the values presented in this work stand for the arithmetic averages of the obtained data.

In the kinetic experiments, 0.025 g of nZVI samples was added into separate 10.0 mL portions of 100.0 mg/L Ni^{2+} solutions, and the mixtures were shaken for 10 min, 30 min, 1 h, 4 h, 8 h, and 24 h contact times.

The effect of the initial Ni^{2+} concentration on the extent of uptake was investigated at 10.0, 25.0, 50.0, 75.0, 100.0, 200.0, 300.0, 400.0, and 500.0 mg/L concentrations. The experiments were performed by adding 0.025 g, 0.050 g, or 0.10 g of nZVI sample into 10.0 mL potions of Ni^{2+} solutions. The mixtures were shaken on the orbital shaker for 4 h prior to centrifugation. The supernatant solutions were then filtered and transferred into clean tubes until AAS analysis.

The experiments investigating the pH effect were conducted after adjusting the initial pH's of the mixtures to 4.0, 6.0, 8.0, or 10.0 using 0.01 M, 0.1 M, or 1.0 M of HNO_3 and NaOH solutions. In each experiment 10.0 mL portions of Ni^{2+} solutions were contacted with 0.025 g nZVI for periods of 4 h. The pH of the solutions was also measured at the end of shaking process.

Part of the experiments was performed to assess the reusability of nZVI materials in successive uptake trials. In each experiment 0.025 g nZVI sample was added into 10.0 mL aliquot of 10.0 mg/L or 100.0 mg/L Ni^{2+} solutions. After shaking periods of 30 min, the mixtures were centrifuged; the supernatant solutions were transferred into new tubes and acidified. Then fresh 10.0 mL aliquots of Ni^{2+} solution were added onto the residual nZVI samples and the mixtures were shaken again for 30 min. These trials were repeated for seven times.

In the desorption tests, 10.0 mL portions of high purity water were added onto the Ni-loaded nZVI samples and were shaken for 24 h. The supernatant solutions were then analyzed for possibly released Ni ions.

A series of experiments was performed to compare the extent of uptake of Ni^{2+} with those of Cd^{2+}, Sr^{2+}, Zn^{2+}, and Cu^{2+} ions. The solutions of these cations were prepared from $CdCl_2$ (Fluka 20899), $Cu(NO_3)_2 \cdot 5/2H_2O$ (Riedel-de Haën 31288), $SrCl_2.6H_2O$ (Merck 393065), and $Zn(NO_3)_2 \cdot 6H_2O$ (Fluka 96482). The experiments were studied at the initial cation concentrations of 10.0, 25.0, 50.0, 75.0, 100.0, 200.0, 300.0, 400.0, and 500.0 mg/L. In each experiment, 0.025 g nZVI dose was contacted with 10.0 mL portions of metal solutions.

3. Results and discussion

3.1. Characterization of nZVI

XRD analysis of freshly synthesized nZVI showed that nZVI is dominated by Fe^0 characterized by its main reflection at 44.9°. Weak signals of iron oxides (hematite, Fe_2O_3 and magnetite, Fe_3O_4) were detected in the nZVI samples after several weeks of storage under ambient conditions. The obtained results are in parallel with the ones we reported earlier for nZVI [4,5]. The presence of Fe and O in the nanoparticles surface is evident in the XPS spectrum given in Fig. 1, which indicates also the presence of some boron (must be originating from NaBH4 used during synthesis). The incorporation of B in the outer shell of Fe nanoparticles was reported earlier to take place in the form of oxidized B (borate) and some reduced B (boride) [16]. This inclusion was suggested as an auxiliary factor in the particle resistance against oxidation by atmospheric attack [17]. The primary reason for the slow oxidation is due to the oxide shell which is reported to be insoluble over the neutral pH conditions [18].

The structure of nZVI was also analyzed using HR-TEM. Typical images of fresh and aged nZVI samples are shown in Fig. 2. The nZVI particles demonstrated the characteristic chain-like structure, with the size of individual particles ranging within 10–60 nm (Fig. 2a). The chain-like morphology leads to decreasing the reactivity of the nanoparticles in terms of the available surface area, but at the same time provides the advantage of easier sorbent-solution phase separation at the end of uptake operation. The well known core-shell

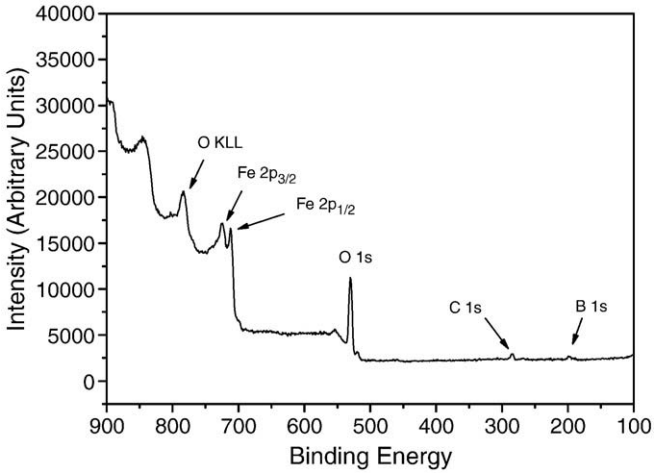

Fig. 1. XPS spectrum of an nZVI sample.

structure of the nanoparticles is shown in Fig. 2b, with the oxide layer appearing to be about 3–5 nm thick. The absence of high resolution lattice fringes in the shell regions suggests that the iron-oxide is amorphous. The structural features of the nanoparticles are in agreement with those given in our earlier results in which the core was reported to be composed of α-Fe [5].

TEM images in Fig. 2c and 2d show nZVI aged for six months. In general, Fe^0 nanoparticles are observed to retain their chain-like morphology, with the thickness of the oxide layer showing slight variation (~5 nm). However, in some regions massive oxidation is observed leading to a different morphology (Fig. 2d).

The zeta potential of nZVI aqueous suspensions was measured at different pH values to determine the Iso-Electric-Point (IEP) of the material. The results indicate that the IEP occur around 8.1–8.2. This value is close to the values reported in literature [19]. It is reported that the given value is higher than those of magnetite (Fe_3O_4) (~6.8) and maghemite (γ-Fe_2O_3) (~6.6), and that no variation or shift of IEP was observed in the aged nZVI samples [19].

According to multiple BET-N_2 analysis, the surface area was around 12–16 m^2 per gram of iron nanoparticles. The surface area measured on a dry basis is unlikely to reflect the actual available area in solution because of the tendency of nZVI particles to aggregate further inside solution [16,20]. Particles size distribution measured for nZVI in water is shown in Fig. 3. According to the analysis, the material tends to form three types of aggregates. While the majority of the nanoparticle chains gather inside water in about 20 μm size aggregates, smaller portions of nZVI chains appear to form what might be described as *short-range* aggregates and long-*range* aggregates

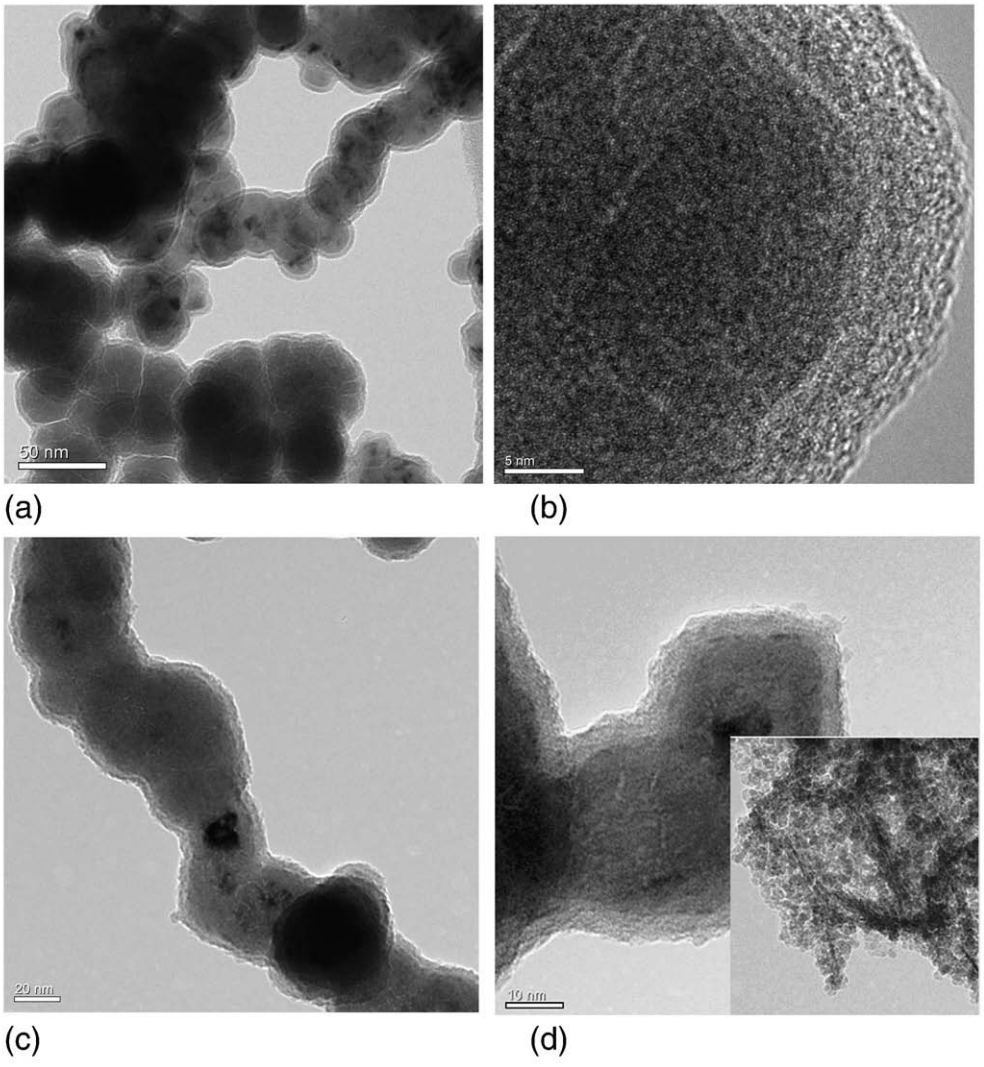

Fig. 2. HR-TEM images of nZVI samples; (a,b) fresh, and (c,d) aged for six months.

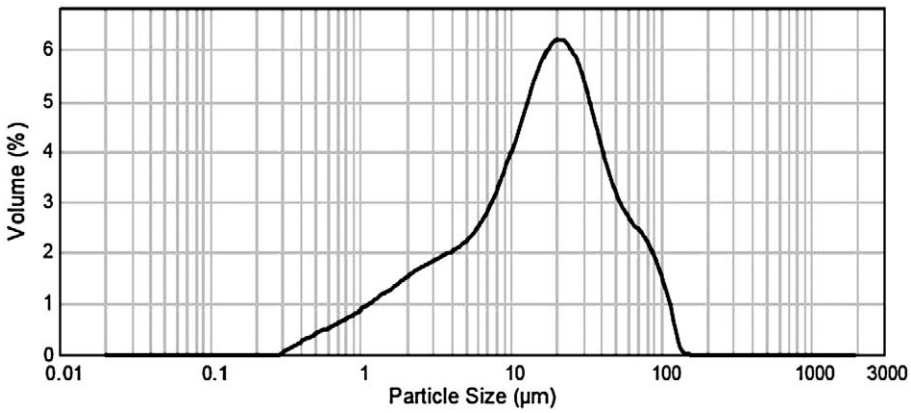

Fig. 3. Particle size distribution of iron nanoparticles in aqueous medium.

peaking around 2 μm and 80 μm, respectively. These values are highly above the ones reported for dry nZVI. However, the stability of these aggregates inside water bodies under different conditions in relation with the nZVI fixation capacity is a topic that requires further elaboration.

3.2. Results of uptake experiments of Ni^{2+} ions

In aqueous solution, transition metals are known to assume different chemical forms that depend on the pH of the medium. The speciation analysis of aqueous Ni^{2+} ions was performed at various input conditions of initial concentration, temperature, pH, and ionic strength values using visual MINTEQ software. The obtained results indicate that Ni ions persist in their divalent forms up to pH value around 8.5. Beyond this, different hydroxyl forms of the ions can be observed depending on the pH. These forms include $Ni(OH)^{+}$, $Ni(OH)_2$, $Ni(OH)_3^{-}$. Within the pH ranges measured in the uptake experiments of this study, the Ni ions are expected to persist dominantly as Ni^{2+}.

Throughout this study, the equilibrium concentration and percentage uptake of Ni^{2+} ions on nZVI were calculated using the mass balance equations:

$$[C]_s = ([C]_0 - [C]_l)(V / M) \quad (1)$$

$$\%\ uptake = ([C]_0 - [C]_l)(1 / [C]_0) \times 100\% \quad (2)$$

where $[C]_s$ is the concentration of Ni^{2+} on nZVI (mg/g), $[C]_l$ is their concentration in liquid solution (mg/L), V is the solution volume (L), and M is the mass of nZVI (g).

The obtained results of the effect of time on the uptake of Ni^{2+} ions on nZVI indicated that, under the studied conditions, the uptake approaches equilibrium in less than one hour of shaking time. The subsequent experiments were performed at mixing time of four hours in order to ensure the attainment of equilibrium.

The variation in the extent of uptake of Ni^{2+} ions as a function of initial concentration at three different doses of nZVI (0.025 g, 0.050 g, or 0.10 g added into 10 mL portions of metal solutions) is shown in Fig. 4. As given in Fig. 4a, the normalized amount of fixed Ni^{2+} (mg Ni/g nZVI) increases with the increase in the initial cation concentration. This increase is seen to level off at higher initial concentrations when 0.025 g nZVI is used, but is almost linear when 0.10 g nZVI is applied. Such a behavior is justified by the increase in the available surface area when nZVI amount is raised. The extent of fixation, in terms of % uptake, for Ni^{2+} at different nZVI doses is also shown in Fig. 4b. A complete removal of Ni^{2+} ions is achievable at all doses up to the initial concentration of 100.0 mg/L. Beyond this concentration a complete removal can still be achieved by increasing the nZVI amount. Within the studied conditions, the capacity of uptake is around 0.08 g Ni/g nZVI.

The effect of pH on the removal of Ni^{2+} ions was studied over the range 4.0 to 10.0. The obtained results expressed as concentrations of Ni^{2+} on nZVI (mg/g) and percentage uptake at different pH values and nZVI amounts are given Table 1. As is seen, the uptake shows an increase with increasing pH at the nZVI amount of 0.025 g. When the

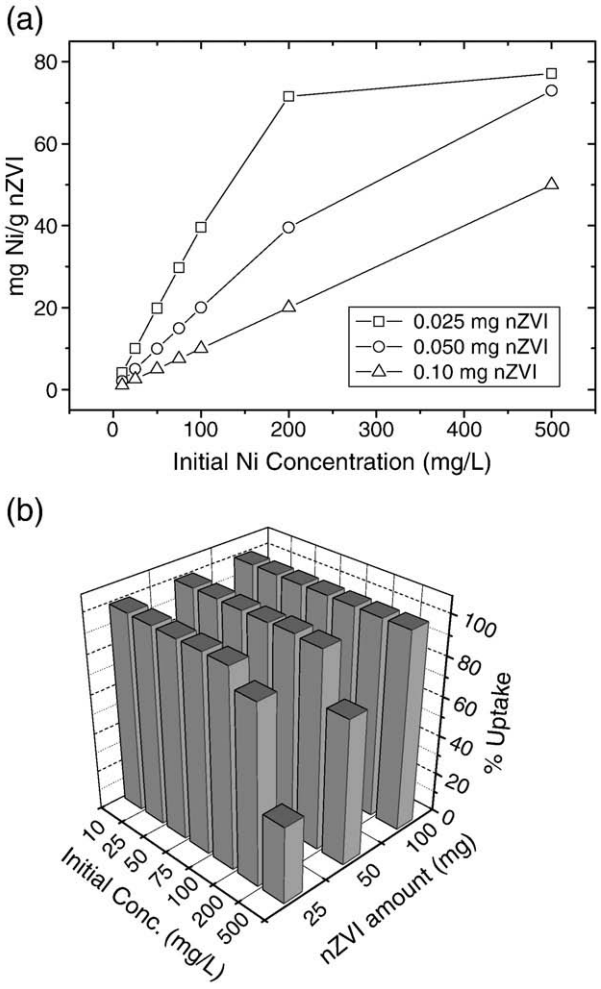

Fig. 4. (a) Variation of the amount of uptake of Ni^{2+} ions with initial concentration, and (b) the variation of % uptake of Ni^{2+} ions with the initial concentration, at different nZVI doses.

Table 1
The equilibrium values corresponding to the uptake of Ni^{2+} ions by nZVI at various initial solution pH values.

pH	0.025 g nZVI			0.05 g nZVI			0.1 g nZVI		
	$[C]_l$ mg/L	$[C]_s$ mg/g	% uptake	$[C]_l$ mg/L	$[C]_s$ mg/g	% uptake	$[C]_l$ mg/L	$[C]_s$ mg/g	% uptake
4.0	16	34	84	0.4	20	>99	0	10	>99.9
6.0	9	36	91	0.8	20	>99	0	10	>99.9
8.0	0	40	>99.9	0	20	>99.9	0	10	>99.9
10.0	0	40	>99.9	0	20	>99.9	0	10	>99.9

amount of nZVI is increased, almost a complete removal of Ni^{2+} ions is achieved at all investigated pH value. It is worth noting that precipitation must have contributed to the uptake at high pH values, in particular, at pH of 10.0.

Other sets of experiments were conducted to evaluate the effect of repetitive application of nZVI samples on their removal capability towards Ni^{2+}. The obtained results for two different nZVI doses, 0.025 mg and 0.050 mg, indicated that the nZVI removal capacity has largely deteriorated after the first cycle of application. This result resembles our earlier observation obtained for Cu^{2+} uptake on nZVI [5], but differs from the one observed for Co^{2+} ions [4].

HR-TEM images of nZVI following the uptake of Ni^{2+} ions are shown in Fig. 5. As demonstrated by the images, nZVI undergo extensive oxidation as a result of exposure to aqueous solution leading to loss of chain-like morphology and formation of what resembled a needle-like structure. The XPS analysis of nZVI after the uptake of Ni^{2+} ions reveals also that the iron nanoparticles had undergone wet oxidation to form iron oxides and oxyhydroxide. The O 1s photoelectron profile, shown in Fig. 6a, displayed a peak centred at 530.7 ± 0.1 eV which was slightly asymmetric to the high binding energy side. Curve fitting of the O 1 s profile indicated that three peaks centred at 530.0 eV, 531.3 eV and 532.9 eV contributed to the overall signal. The predominant signal contribution was attributed to O^{2-} in metal oxides (44%) with a similar contribution (40% by area) attributed to structural OH^- in solid hydroxide phases that could be stemming from either FeO(OH) or $Ni(OH)_2$. The peak fitted at 532.9 eV is characteristic of physi-sorbed water and accounted only to 16% of the signal contribution.

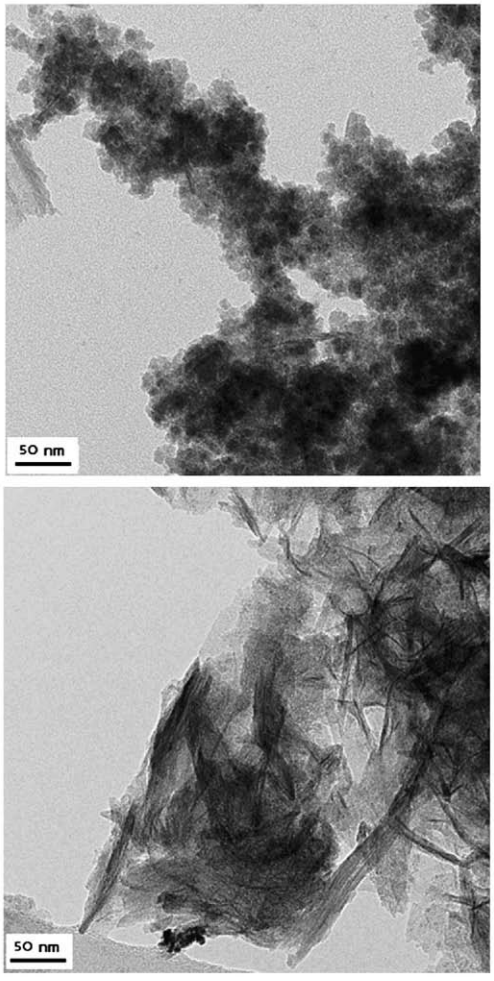

Fig. 5. HR-TEM images of nZVI samples following the uptake of Ni^{2+} ions.

The recorded Fe 2p photoelectron profile, Fig. 6b, was very similar to that previously reported for Fe in iron oxyhydroxide (FeOOH) [21,22], with the Fe $2p_{3/2}$ line centred at 711.6 ± 0.1 eV binding energy.

Based on an XPS investigation of Ni^{2+} fixation by nZVI from a mechanistic aspect, it was suggested that Ni^{2+} ions are initially bound to the outer shell of nZVI by surface complexation, and is subsequently reduced to metallic Ni on the nanoparticle surface [15]. In another study, it was reported that both metallic and ionic forms of Ni were present on nZVI surface [7]. The XPS features obtained in this study for Ni on nZVI at an initial concentration of 1000 mg/L are given in Fig. 6c. The Ni $2p_{3/2}$ peak is centred at the binding energy of 855.95 ± 0.1 eV. This value lies far from the one of the Ni $2p_{3/2}$ line of metallic nickel well reported to occur at 852.8 ± 0.2 eV [23,24]. The measured value seems to be close to the binding energy of the Ni $2p_{3/2}$ line reported for Ni^{2+} in NiO at 854.4 ± 0.2 eV [24,25], and for Ni^{2+} in $Ni(OH)_2$, reported at 855.6 eV [26,27] to 856.0 eV [28]. This is probably indicating that, at the investigated high loading, Ni^{2+} ions tend to be fixed on nZVI mainly by surface precipitation rather than a redox mechanism. In addition, although Ni^{2+} possesses a more positive standard reduction potential (−0.24 V @ 298 K) than that of Fe^{2+} (−0.44 V @ 298 K), it might not entirely undergo reduction by Fe^0 core. A possible justification is that in the course of indirect electron transfer (from the core through the shell of to the external surface of the nanoparticle [7]), the given reduction potential of Ni might overlap with the Fermi level of oxide shell (reported to vary within −0.18 to −0.33 V [29]). The fixation mechanisms on nZVI in relation to the energy of the conduction band of iron oxide shell were previously discussed for various cations in a study by Li and Zhang [7].

3.3. Further uptake experiments involving Cu^{2+}, Cd^{2+}, Zn^{2+}, and Sr^{2+} ions

Further experiments were performed to compare the extent of retention of Ni^{2+} to those of Cu^{2+}, Cd^{2+}, Zn^{2+}, and Sr^{2+} under identical conditions. These cations belong to a wide range of reduction potentials as given in Table 2. The experiments attempted to elucidate any possible correlations between the standard reduction potentials of these ions and their extent of uptake. For Sr^{2+}, an alkaline earth metal ion, the standard reduction potential is much smaller than that of Fe^{2+} and thus its reduction by nZVI is not expected. Cu^{2+}, on the other hand, possesses a standard reduction potential well above that of Fe^{2+} and its reduction was documented in a previous study carried out at our laboratories [5]. The standard reduction potential of Cd^{2+} and Zn^{2+} lie in between. In addition to standard electrode potential,

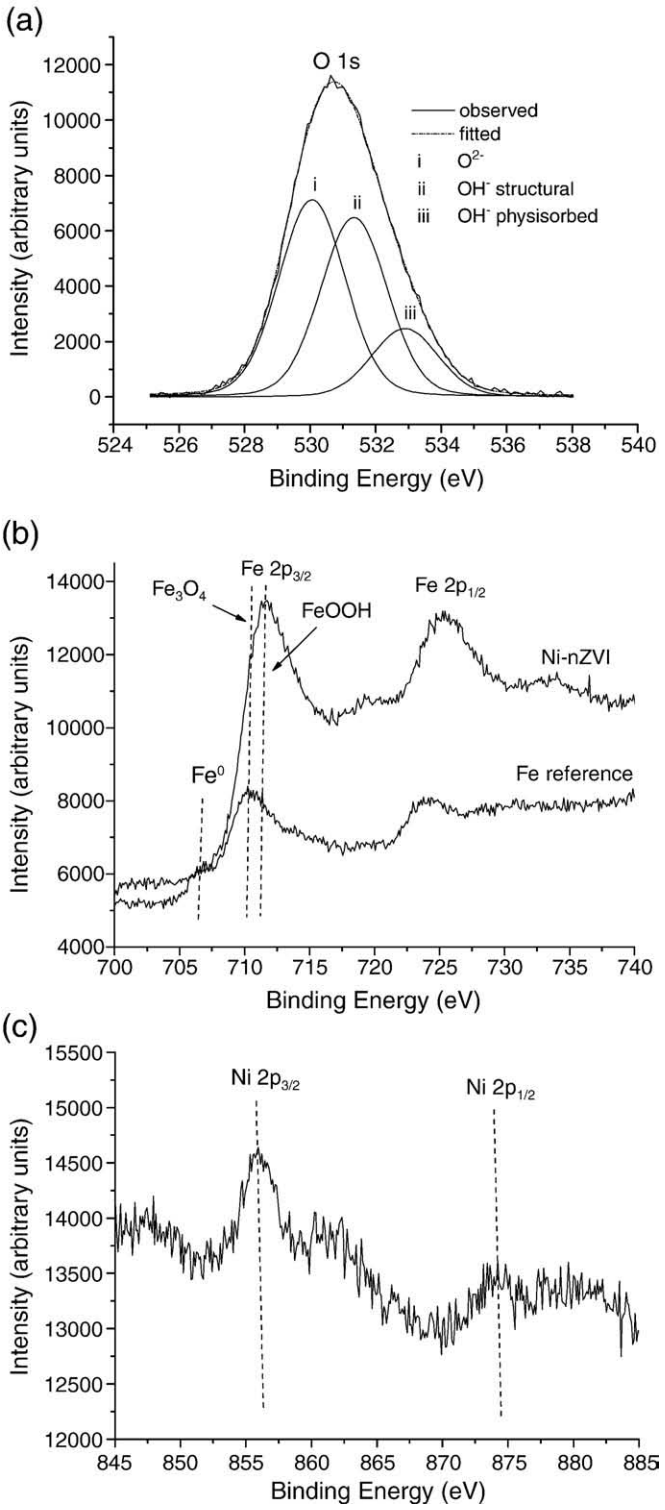

Fig. 6. XPS spectra obtained from a Ni-loaded nZVI sample: (a) O 1s, (b) Fe 2p, and (c) Ni 2p.

another property that might be essential in defining the extent of uptake is the charge density (charge/size) of the ions. This property relates with the sorption behavior of the cations by the external hydroxyl groups on the nanoparticle surface. The sizes of the above ions are provided in Table 3 at their smallest and highest coordination numbers.

The comparative investigations included elucidating the effects of time, concentration, in addition to desorption tests. The results of the kinetic experiments are shown in Fig. 7. All the four transition metal ions; Cu^{2+}, Cd^{2+}, Zn^{2+}, and Ni^{2+} approached equilibrium very rapidly, whereas the uptake of the alkaline earth metal cation Sr^{2+} continued to increase over the studied period. The exceptional behavior of Sr^{2+} persists also when the effect of concentration is studied. A set of loading experiments were performed within the initial concentration range of 10.0–100.0 mg/L and the results are given in Table 4. According to the data, Sr^{2+} ions appear as the least preferred ones by nZVI. The principal reason for the exceptional behavior of Sr^{2+} might be its significantly lower charge density of Sr^{2+} in comparison with the others. As is known, the charge density is an important factor to look at when complexation reactions (or inner-sphere complex formation between fixed cation and hydroxide groups on the surface of iron nanoparticles) are considered. For the other cations, the difference in % uptake between the four transitions metal ions is not significant up to the initial concentration of 100.0 mg/L. The similarity might be referred to the resemblance of chemical nature among these ions and relatively close charge densities. At the initial concentration of 100.0 mg/L, the priority of fixation of the studied cations by nZVI

Table 2
Standard electrode potentials at 25 °C, [30].

Element	Half-cell reaction	E^0 (V)
Strontium (Sr)	$Sr^{2+} + 2\,e^- \rightarrow Sr$	−2.89
Zinc (Zn)	$Zn^{2+} + 2\,e^- \rightarrow Zn$	−0.76
Iron (Fe)	$Fe^{2+} + 2\,e^- \rightarrow Fe$	−0.44
Cadmium (Cd)	$Cd^{2+} + 2\,e^- \rightarrow Cd$	−0.40
Nickel (Ni)	$Ni^{2+} + 2\,e^- \rightarrow Ni$	−0.23
Copper (Cu)	$Cu^{2+} + 2\,e^- \rightarrow Cu$	+0.34

Table 3
The radii of cations (Shannon Radii) at their smallest and highest coordination numbers (CN), [31].

Cation	Radius (pm)
Sr^{2+}	118 at CN of VI 144 at CN of XII
Ni^{2+}	55 at CN of IV 69 at CN of VI
Cu^{2+}	57 at CN of IV 73 at CN of VI
Zn^{2+}	60 at CN of IV 90 at CN of VIII
Cd^{2+}	78 at CN of IV 131 at CN of XII

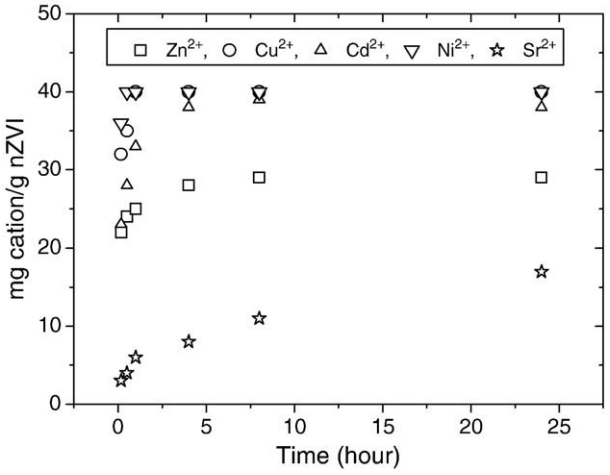

Fig. 7. Variation of the amount of the ions fixed by nZVI with the contact time.

Table 4
Effect of initial cation concentration on the % uptake of various cations by nZVI.

Initial conc.	% Uptake				
(mg/L)	Cd^{2+}	Ni^{2+}	Zn^{2+}	Cu^{2+}	Sr^{2+}
10.0	>99.9	>99.9	>99.9	>99.9	77
25.0	99	99.6	>99.9	>99.9	52
50.0	99	99	>99.9	>99.9	44
75.0	99	99	99	>99.9	40
100.0	95	97	70	>99.9	43

follows the order: $Cu^{2+} > Ni^{2+} > Cd^{2+} > Zn^{2+} > Sr^{2+}$. This priority order follows the standard reduction potential order of the cations. However, this observation was not obeyed when further experiments were performed at higher initial concentrations of the cations. The results, given in Table 5 indicate that the highest uptake is achieved in the case of Ni^{2+} ions and that the uptake of Zn^{2+} becomes comparable to that of Cd^{2+} and Cu^{2+} ions which possess higher standard reduction potentials than Zn^{2+} ions. The decrease in Cu^{2+} retention at higher concentrations might be attributed to the formation of Cu_2O and Cu^0 on the surface of nZVI [5], in a way that restricts the interaction of further Cu^{2+} ions with nZVI surface.

At higher loadings, it seems that the charge density of the cation becomes increasingly effective in determining the extent of uptake of the studied cations. This could be related with the better ability of smaller cations to diffuse and form inner-sphere complexes (binding of cations to inner oxygen atoms in oxyhydroxyl groups in the oxide shell).

The desorption behavior of the cations was also studied in order to test the stability of uptake. The results, provided in Table 6, indicate that the uptake of the four transition metal cations appears to be very stable, with only minimal amounts released at the end of the desorption period (24 h). On the other hand, Sr^{2+} uptake appears to be highly unstable possibly pointing to an outer-sphere complex formation. The stability of Cu fixation might be explained by the oxidation–reduction mechanism that leads to irreversible transformation of Cu^{2+} ions into metallic Cu and Cu_2O [5]. For the other transition metals, the high stability of uptake could be stemming from an inner-sphere complex formation with the oxyhydroxyl groups on nZVI surface.

The overall results demonstrate the high fixation capability and fast uptake kinetics of nZVI towards transition metal ions, but nevertheless, raise a question mark on the suitability of nZVI for the removal of alkaline earth cations. Further work is required in this regard.

Table 5
Effect of high initial cation concentrations on the % uptake of studied transition metal cations by nZVI.

Initial conc.	% Uptake			
(mg/L)	Cd^{2+}	Ni^{2+}	Zn^{2+}	Cu^{2+}
200.0	47	90	60	65
300.0	25	43	20	42
400.0	22	33	15	23
500.0	18	31	16	16

Table 6
The % desorption of studied cations loaded previously on nZVI at different initial concentrations.

Initial conc.	% Desorption				
(mg/L)	Cd^{2+}	Ni^{2+}	Zn^{2+}	Cu^{2+}	Sr^{2+}
10.0	0	0	0	0	63
25.0	0	0	0	0	60
50.0	0	0	0	0	41
100.0	<1	0	0	0	33
200.0	9	1	3	0	35
500.0	47	25	10	0	16

4. Conclusions

Over the studied contact times and initial concentrations, nZVI demonstrated a high potential towards uptake of aqueous Ni^{2+} ions in terms of fast kinetics and high uptake capacity. XPS results suggested that Ni^{2+} ions are fixed mainly in their divalent form possibly through complexation and surface precipitation. The extent of uptake was not seriously affected by pH variations in the range 4.0 to 10.0.

The results obtained for the studied other cations revealed high uptake capacities, fast uptake kinetics, and very limited desorption of initially fixed transition metal ions from nZVI. The same was, however, not observed for Sr^{2+} ions.

Acknowledgement

The authors thank Dr. K. R. Hallam and Dr. T. B. Scott at the Interface Analysis Centre, University of Bristol for their help in XPS analysis. The authors are grateful also to the Center of Materials Research at İZTECH for the help in SEM/EDX and BET-N_2 analysis.

References

[1] W.-X. Zhang, Nanopart Res. 5 (2003) 323.
[2] D.L. Huber, Small 1 (2005) 482.
[3] L. Li, M. Fan, R.C. Brown, J.V. Leeuwen, J. Wang, W. Wang, Y. Song, P. Zhang, Crit. Rev. Environ. Sci. Technol. 36 (2006) 405.
[4] Ç. Üzüm, T. Shahwan, A.E. Eroğlu, I. Lieberwirth, T.B. Scott, K.R. Hallam, Chem. Eng. J. 144 (2008) 213.
[5] D. Karabelli, C. Uzum, T. Shahwan, A.E. Eroglu, T. Scott, K.R. Hallam, I. Lieberwirth, Ind. Eng. Chem. Res. 47 (2008) 4758.
[6] Ç. Üzüm, T. Shahwan, A.E. Eroğlu, K.R. Hallam, T.B. Scott, I. Lieberwirth, Appl. Clay Sci. 43 (2009) 172.
[7] X.-Q. Li, W.-X. Zhang, J. Phys. Chem. C. 111 (2007) 6939.
[8] S.M. Ponder, J.G. Darab, T.E. Mallouk, Environ. Sci. Technol. 34 (2000) 2564.
[9] S.R. Kanel, J.M. Greneche, H. Choi, Environ. Sci. Technol. 40 (2006) 2045.
[10] Y. Xu, D. Zhao, Water Res. 41 (2007) 2101.
[11] K-H. Shin, D.K. Cha, Chemosphere 72 (2008) 257.
[12] G.C.C. Yang, H-L. Lee, Water Res. 39 (2005) 884.
[13] V.T. Nguyen, S. Vigneswaran, H.H. Ngo, H.K. Shon, J. Kandasamy, Desalination 236 (2009) 363.
[14] H. Genç-Fuhrman, P. Wu, Y. Zhou, A. Ledin, Desalination 226 (2008) 357.
[15] X.Q. Li, W.-X. Zhang, Langmuir 22 (2006) 4638.
[16] J.T. Nurmi, P.G. Tratnyek, V. Sarathy, D.R. Bear, J.E. Amonette, K. Peacher, C. Wang, J.C. Linehan, D.W. Matson, R.L. Penn, M.D. Driessen, Environ. Sci. Technol. 39 (2005) 1221.
[17] S.M. Ponder, J.G. Darab, J. Bucher, D. Caulder, L. Craig, L. Davis, N. Edelstein, W. Lukens, H. Nitsche, L. Rao, D.K. Shuh, T.E. Mallouk, Chem. Mater. 13 (2001) 479.
[18] X-q. Li, D.W. Elliott, W-x. Zhang, Crit. Rev. Solid State Mater. Sci. 31 (2006) 111.
[19] Y-P. Sun, X-q. Li, J. Cao, W-x. Zhang, H.P. Wang, Adv. Colloid. Interfac. 120 (2006) 47.
[20] G.C.C. Yang, H-C. Tu, C-H. Hung, Sep. Purif. Technol. 58 (2007) 166.
[21] K. Kishi, T. Fujita, Surf. Sci. 227 (1990) 107.
[22] N.S. McIntyre, D.G. Zetaruk, Anal. Chem. 49 (1977) 1521.
[23] N.S. McIntyre, M.G. Cook, Anal. Chem. 47 (1975) 2208.
[24] C.D. Wagner, W.M. Riggs, L.E. Davis, J.F. Moulder, G.E. Muilenberg, Handbook of X-Ray Photoelectron Spectroscopy, Perkin-Elmer Corporation, Physical Electronics Division, Minn. 55344: Eden Prairie, 1979.
[25] K. Kishi, J. Electron Spectrosc. Relat. Phenom. 46 (1988) 237.
[26] N.S. McIntyre, M.G. Cook, Anal. Chem. 47 (1975) 2208.
[27] P. Lorenz, J. Finster, G. Wendt, J.V. Salyn, E.K. Zumadilov, V.I. Nefedov, J. Electron Spectrosc. Relat. Phenom. 16 (1979) 267.
[28] C.P. Li, A. Proctor, D.M. Hercules, Appl. Spectrosc. 38 (1984) 880.
[29] B.A. Balko, P.G. Tratnyek, J. Phys. Chem. B 102 (1998) 1459.
[30] P. Atkins, J. De Paula, Atkins' Physical Chemistry8th edition, Oxford Press, 2006.
[31] http://abulafia.mt.ic.ac.uk/shannon/ptable.php (last access date 08/04/2008).